Removal of surface-reflected light for the measurement of remote-sensing reflectance from an above-surface platform

ZhongPing Lee,[1,*] Yu-Hwan Ahn,[2] Curtis Mobley,[3] and Robert Arnone[4]

[1]Geosystems Research Institute, Mississippi State University Stennis Space Center, Mississippi 39529, USA
[2]Korea Ocean Research & Development Institute Ansan, P.O. Box 29, 425-600, Korea
[3]Sequoia Scientific, Inc. 2700 Richards Road, Suite 107, Bellevue, Washington 98005, USA
[4]Naval Research Laboratory Stennis Space Center, Mississippi 39529, USA
*zplee@ngi.msstate.edu

Abstract: Using hyperspectral measurements made in the field, we show that the effective sea-surface reflectance ρ (defined as the ratio of the surface-reflected radiance at the specular direction corresponding to the downwelling sky radiance from one direction) varies not only for different measurement scans, but also can differ by a factor of 8 between 400 nm and 800 nm for the same scan. This means that the derived water-leaving radiance (or remote-sensing reflectance) can be highly inaccurate if a spectrally constant ρ value is applied (although errors can be reduced by carefully filtering measured raw data). To remove surface-reflected light in field measurements of remote sensing reflectance, a spectral optimization approach was applied, with results compared with those from remote-sensing models and from direct measurements. The agreement from different determinations suggests that reasonable results for remote sensing reflectance of clear blue water to turbid brown water are obtainable from above-surface measurements, even under conditions of high waves.

©2010 Optical Society of America

OCIS codes: (010.4450) Ocean optics; (280.0280) Remote sensing.

References and links

1. A. Morel, "In-water and remote measurements of ocean color," Boundary-Layer Meteorol. **18**(2), 177–201 (1980).
2. S. B. Hooker, G. Lazin, G. Zibordi, and S. D. McLean, "An Evaluation of Above- and In-Water Methods for Determining Water-Leaving Radiances," J. Atmos. Ocean. Technol. **19**(4), 486–515 (2002).
3. G. Zibordi, B. Holben, S. B. Hooker, F. Mélin, J.-F. Berthon, and I. Slutsker, "A network for standardized ocean color validation measurements," Eos Trans. AGU **87**(293), 297 (2006).
4. G. Zibordi, S. B. Hooker, J. F. Berthon, and D. D Alimonte, "Autonomous Above-Water Radiance Measurements from an Offshore Platform: A Field Assessment Experiment," J. Atmos. Ocean. Technol. **19**(5), 808–819 (2002).
5. S. B. Hooker, G. Zibordi, J.-F. Berthon, and J. W. Brown, "Above-water radiometry in shallow coastal waters," Appl. Opt. **43**(21), 4254–4268 (2004).
6. R. C. Smith, C. R. Booth, and J. L. Star, "Oceanographic biooptical profiling system," Appl. Opt. **23**(16), 2791–2797 (1984).
7. D. A. Toole, D. A. Siegel, D. W. Menzies, M. J. Neumann, and R. C. Smith, "Remote-sensing reflectance determinations in the coastal ocean environment: impact of instrumental characteristics and environmental variability," Appl. Opt. **39**(3), 456–469 (2000).
8. J. L. Mueller, and R. W. Austin, eds., *Ocean Optics Protocols for SeaWiFS Validation, Revision 1*, NASA Tech. Memo. 104566 (NASA, Goddard Space Flight Center, Greenbelt, Maryland, 1995), Vol. 25, p. 67.
9. K. L. Carder, and R. G. Steward, "A remote-sensing reflectance model of a red tide dinoflagellate off West Florida," Limnol. Oceanogr. **30**(2), 286–298 (1985).
10. J. L. Mueller, C. Davis, R. Arnone, R. Frouin, K. L. Carder, Z. P. Lee, R. G. Steward, S. Hooker, C. D. Mobley, and S. McLean, "Above-water radiance and remote sensing reflectance measurement and analysis protocols," in *Ocean Optics Protocols for Satellite Ocean Color Sensor Validation, Revision 3, NASA/TM-2002–210004*, J. L. Mueller and G. S. Fargion, eds. (2002), pp. 171–182.

11. G. Zibordi, F. Mélin, S. B. Hooker, D. D'Alimonte, and B. Holben, "An Autonomous Above-Water System for the Validation of Ocean Color Radiance Data," IEEE Trans. Geosci. Rem. Sens. **42**(2), 401–415 (2004).
12. G. Zibordi, J.-F. Berthon, F. Mélin, D. D'Alimonte, and S. Kaitala, "Validation of satellite ocean color primary products at optically complex coastal sites: Northern Adriatic Sea, Northern Baltic Proper and Gulf of Finland," Remote Sens. Environ. **113**(12), 2574–2591 (2009).
13. C. D. Mobley, "Estimation of the remote-sensing reflectance from above-surface measurements," Appl. Opt. **38**(36), 7442–7455 (1999).
14. R. W. Austin, "Inherent spectral radiance signatures of the ocean surface," in *Ocean Color Analysis*, S. W. Duntley, ed. (Scripps Inst. Oceanogr., San Diego, 1974), pp. 1–20.
15. R. G. Steward, K. L. Carder, and T. G. Peacock, "High resolution in water optical spectrometry using the Submersible Upwelling and Downwelling Spectrometer (SUDS)," presented at the EOS AGU-ASLO, San Diego, CA, February 21–25, 1994.
16. A. Morel, and S. Maritorena, "Bio-optical properties of oceanic waters: A reappraisal," J. Geophys. Res. **106**(C4), 7163–7180 (2001).
17. R. C. Smith, and K. S. Baker, "Optical properties of the clearest natural waters (200-800 nm)," Appl. Opt. **20**(2), 177–184 (1981).
18. G. Zibordi, B. Holben, I. Slutsker, D. Giles, D. D'Alimonte, F. Melin, J.-F. Berthon, D. Vandemark, H. Feng, G. Schuster, B. E. Fabbri, S. Kaitala, and J. Seppala, "AERONET-OC: A network for the validation of ocean color primary products," J. Atmos. Ocean. Technol. **26**(8), 1634–1651 (2009).
19. Z. P. Lee, K. L. Carder, R. G. Steward, T. G. Peacock, C. O. Davis, and J. L. Mueller, "Remote-sensing reflectance and inherent optical properties of oceanic waters derived from above-water measurements," presented at the Ocean Optics XIII, 1996.
20. Z. P. Lee, K. L. Carder, R. Arnone, and M. He, "Determination of primary spectral bands for remote sensing of aquatic environments," Sensors (Basel Switzerland) **7**(12), 3428–3441 (2007).
21. C. S. Roesler, and M. J. Perry, "In situ phytoplankton absorption, fluorescence emission, and particulate backscattering spectra determined from reflectance," J. Geophys. Res. **100**(C7), 13279–13294 (1995).
22. Z. P. Lee, K. L. Carder, C. D. Mobley, R. G. Steward, and J. S. Patch, "Hyperspectral remote sensing for shallow waters. 2. Deriving bottom depths and water properties by optimization," Appl. Opt. **38**(18), 3831–3843 (1999).
23. R. Doerffer, and J. Fischer, "Concentrations of chlorophyll, suspended matter, and gelbstoff in case II waters derived from satellite coastal zone color scanner data with inverse modeling methods," J. Geophys. Res. **99**(C4), 7457–7466 (1994).
24. S. Maritorena, D. A. Siegel, and A. R. Peterson, "Optimization of a semianalytical ocean color model for global-scale applications," Appl. Opt. **41**(15), 2705–2714 (2002).
25. E. Devred, S. Sathyendranath, V. Stuart, H. Maass, O. Ulloa, and T. Platt, "A two-component model of phytoplankton absorption in the open ocean: Theory and applications," J. Geophys. Res. **111**, C03011 (2006), doi:03010.01029/02005JC002880.
26. Z. Lee, K. L. Carder, R. F. Chen, and T. G. Peacock, "Properties of the water column and bottom derived from Airborne Visible Infrared Imaging Spectrometer (AVIRIS) data," J. Geophys. Res. **106**(C6), 11639–11651 (2001).
27. Y.-H. Ahn, J.-H. Ryu, and J.-E. Moon, "Development of redtide & water turbidity algorithms using ocean color satellite," KORDI Report No. BSPE 98721–00–1224–01, KORDI, Seoul, Korea (1999).
28. A Microsoft Excel template of this processing scheme is available for interested practitioners.

1. Introduction

The remote-sensing reflectance of water (R_{rs}, sr^{-1}) is defined as the ratio of the water-leaving spectral radiance (L_W, W m^{-2} nm^{-1} sr^{-1}) to downwelling spectral irradiance just above the surface ($E_d(0^+)$, W m^{-2} nm^{-1}). R_{rs} (or L_W) is the basis for development of remote-sensing algorithms as well as for satellite sensor vicarious calibration [1–3]. Because of various technique limitations and the random motion of the water surface, accurate determination of R_{rs} remains a challenge [2–5]. The measurement of R_{rs} in marine environments usually involves one of these approaches: 1) measure the vertical distributions of upwelling radiance ($L_u(z)$) and downwelling irradiance ($E_d(z)$) within the water, and then propagate these measurements upward across the sea surface to calculate R_{rs} [6]; 2) use one sensor to measure L_u a few centimeters below the surface and use another sensor to measure $E_d(0^+)$ above the surface, and then propagate L_u across the surface to calculate R_{rs} [7]; 3) measure all relevant quantities from an above-surface platform [1–5,8–12], and then calculate L_W (or R_{rs}) by removing surface-reflected light (L_{SR}). This third approach is widely used in the field and for continuous measurements [3,4,11,12], although each approach has its own advantages and disadvantages [2,10].

When measurements are made from above the sea surface [see Fig. 1(a)], the measured signal is the total upwelling radiance (L_T), which is the sum of the water-leaving radiance (L_W) and the surface-reflected radiance (L_{SR}). It is necessary to avoid viewing surface foam, the shadow of the platform structure, and obvious solar glint spots. Some surface-reflected light (mostly from downwelling sky radiance, but possibly including some sun glint) is inevitable, however. A correction is therefore required to remove the surface-reflected light from L_T in order to compute L_W and R_{rs} [2,4,8]. One approach to the removal of surface-reflected radiance was proposed by Mobley [13] (a similar description can be found in Morel [1]). In this technique, all L_{SR} is expressed as the product of ρ – an effective surface reflectance – and sky radiance (L_{Sky}) measured for an angle reciprocal to the measurement of L_T (see Fig. 1 in Ref. [13]). The value of ρ depends on sea state, sky conditions, and viewing geometry [13,14]. Two approaches have then been proposed for the determination of ρ: One is to derive the value of ρ from measured L_T and L_{Sky} by assuming L_W approaches 0 at near-infrared wavelengths (e.g. at 780 nm) [1]; the other is to use a table of ρ values derived from numerical simulations with various wind speeds and viewing geometries [13]. Both approaches [1,13], however, assume that the ρ value is spectrally constant. To minimize the impact of sun glint on the derivation of L_W (or R_{rs}), Hooker et al. [2] and Zibordi et al. [4] suggested filtering out the higher measured total radiance (L_T) values, and reasonably good results were achieved for L_W in the 412–555 nm range (larger uncertainties were found at 670 nm [4]). Here, after describing the general dependence of ρ, we show with hyperspectral measurements that ρ in general varies with wavelength, and that the spectral variation can be significant. We further compare two physical-mathematical approaches and a direct measurement scheme for the removal of L_{SR} in deriving R_{rs}.

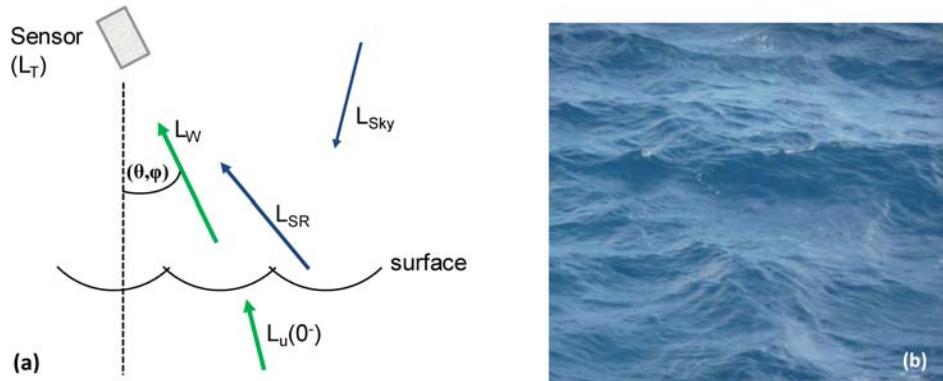

Fig. 1. (a) Schematic illustration of above-surface measurement of L_T. (b) Example of roughened sea surface when looking down from an above-surface platform. The different shades of blue result from light reflected from different parts of the sky.

2. Theoretical background

When a radiance instrument takes measurements of spectral upwelling radiance ($L_T(\lambda)$) from an above-surface platform, it collects not only the radiance emerging from below the water surface (the so-called water leaving radiance, $L_W(\lambda)$), but also surface-reflected light ($L_{SR}(\lambda)$). If the measurement angle is θ from nadir and φ (azimuth) from the solar plane [see Fig. 1(a)], then for a level sea surface, $L_{SR}(\lambda)$ comes from the zenith angle θ' = θ and the same azimuthal angle (φ). For the more common situation of a constantly moving, roughened, surface (see Fig. 1(b) for an example), and for typical instrument integration times of order of one second or longer (integration time is much shorter for multiband sensors [3]), $L_{SR}(\lambda)$ actually comes from a large portion of the sky (see Fig. 1 and Fig. 2 of Mobley [13]) and may include solar radiance (sun glint). So, in general, the spectral upwelling radiance measured from an angular geometry (θ,φ) is

$$L_T(\lambda,\theta,\varphi) = L_W(\lambda,\theta,\varphi) + \sum_i w_i \, F(\theta_i',\varphi_i',\theta,\varphi) \, L_{Sky}(\lambda,\theta_i',\varphi_i'). \tag{1}$$

Here subscript "i" represents the ith small wave facet viewed by the sensor; w_i is the relative weighting of solid angle of the ith facet to the sensor's field-of-view solid angle; F is the Fresnel reflectance of the ith facet; and L_{Sky} is the downwelling radiance incident onto the ith facet, which is reflected into senor's viewing angle.

   Because $L_{SR}(\lambda)$ is assembled in an unknown manner according to Eq. (1), removal of $L_{SR}(\lambda)$ becomes a challenge in the field when measurements are taken from above the sea surface (or sea-surface remote sensing in analogy to satellite remote sensing). For this removal, to a first order approximation, Eq. (1) is simplified as [1,13]

$$L_T(\lambda,\theta,\varphi) = L_W(\lambda,\theta,\varphi) + \rho(\theta,\varphi) \, L_{Sky}(\lambda,\theta',\varphi). \tag{2}$$

Here $L_{Sky}(\theta',\varphi)$ is the sky radiance in the same plane as that of L_T, but with θ' the reciprocal (specular) angle of θ [2,4,8,9]. $\rho(\theta,\varphi)$ is the effective surface reflectance that accounts for reflected sky light from all directions for the given sensor direction, and is assumed to be independent of wavelength. $\rho(\theta,\varphi)$ equals the Fresnel reflectance of the sea surface only if the surface is flat (without waves). Values of $\rho(\theta,\varphi)$ for various viewing directions, sun zenith angles, and wind speeds were evaluated with numerical simulations in [13]. Based on these simulations, it was suggested to use $\theta = 40°$ from the nadir and $\varphi = 135°$ from the sun to minimize L_{SR} when measuring R_{rs} in the field.

   Comparing Eqs. (1) and (2) gives

$$\rho(\theta,\varphi) = \frac{\sum_i w_i \, F(\theta_i',\varphi_i',\theta,\varphi,) \, L_{Sky}(\lambda,\theta_i',\varphi_i')}{L_{Sky}(\lambda,\theta',\varphi)}, \tag{3a}$$

or,

$$\rho(\theta,\varphi) = \frac{L_T(\lambda,\theta,\varphi) - L_w(\lambda,\theta,\varphi)}{L_{Sky}(\lambda,\theta',\varphi)}. \tag{3b}$$

Because L_{Sky} in general has different spectral shapes for different directions [1] (e.g., for a clear sky at noon, L_{Sky} from the horizon appears whiter than that from the zenith), ρ in Eq. (2) or Eq. (3a) will in general be spectrally dependent, especially when solar light is inevitably reflected into sensor's viewing angle by roughened surface, unless the sky is completely overcast.

3. Data and methods

To demonstrate the spectral variation of ρ, hyperspectral measurements over clear oceanic waters were utilized, where the contribution of water to L_T is negligible in the longer wavelengths. The measurements were made on Feb. 23, 1997 around 12:50 pm (local time), for waters near Hawaii at 21.33 N, 158.16 W. The sky was clear with no clouds, the water appeared blue, the wind speed was around 8 m s^{-1}, and the surface wave amplitude was ~2 to 3 feet (~1 m).

   Upwelling total radiance (L_T, 9 scans), downwelling sky radiance (L_{Sky}, 5 scans), and "gray-card" radiance (L_G, 3 scans) reflected from a standard diffuse reflector (Spectralon®) were measured with a handheld spectroradiometer (SPECTRIX [15]), which covers a spectral range ~360 – 900 nm with a spectral resolution ~2 nm and has an integration time about 1.5 seconds for the collection of L_T. The orientation to measure L_T was 30° from nadir and 90° from the solar plane. L_{Sky} was measured in the same plane as L_T, but at an angle 30° from zenith. Downwelling irradiance was determined by assuming that the Spectralon is a lambertian reflector, so that $E_d = \pi L_G/R_G$, with L_G the average of the three scans and R_G the

reflectance of the diffuse reflector (~10%). The measurement was taken at the bow of a large ship with a sensor to water-surface distance about 5 meters. The SPECTRIX has a 10° field of view, which then observed a surface area of ~1 m^2 for this setup.

To evaluate the value and variations of the effective surface reflectance (ρ), Eq. (2) is converted to reflectances, where the total remote-sensing reflectance (T_{rs}, ratio of L_T to E_d) and sky remote-sensing reflectance (S_{rs}, ratio of L_{Sky} to E_d) were calculated for each L_T and L_{Sky} scan, respectively. From Eq. (2), these T_{rs}, R_{rs}, and S_{rs} are related as

$$T_{rs}(\lambda,\theta,\varphi) = R_{rs}(\lambda,\theta,\varphi) + \rho(\theta,\varphi)\,S_{rs}(\lambda,\theta',\varphi),\qquad(4a)$$

or

$$R_{rs}(\lambda,\theta,\varphi) = T_{rs}(\lambda,\theta,\varphi) - \rho(\theta,\varphi)\,S_{rs}(\lambda,\theta',\varphi).\qquad(4b)$$

Further, ρ is calculated as

$$\rho(\theta,\varphi) = \frac{T_{rs}(\lambda,\theta,\varphi) - R_{rs}(\lambda,\theta,\varphi)}{S_{rs}(\lambda,\theta',\varphi)}.\qquad(5)$$

For the calculation of ρ, $R_{rs}(\lambda,30°,90°)$ (assumed equal to $R_{rs}(\lambda,0°,0°)$, and for λ in a range of 400 – 800 nm) was estimated with the bio-optical model of Morel and Maritorena [16] and using a chlorophyll-a concentration of Chl = 0.05 mg m^{-3}, which is an estimate based on observations of MODIS for these waters in February. The model coefficients of Morel and Maritorena [16] cover wavelengths up to 700 nm. For the study here, the model coefficients of wavelengths greater than 700 nm are considered the same as that at 700 nm, except for the attenuation coefficient of pure water, which was replaced with the absorption coefficient of clear natural water [17].

4. Results

4.1 Variation of ρ

For this station, T_{rs} and S_{rs} are presented in Figs. 2(a) and 2(b), respectively. Because the sea surface is roughened by waves, as commonly encountered in the field, we did not get identical T_{rs} for the 9 independent measurements of L_T. This is because each L_T measurement observed a different sea surface, hence a different sky coverage, and thus a different L_{SR}. Nor did we get identical measurements of the 5 S_{rs} because the boat was also constantly moving, and thus the sensor could not maintain the exactly same angular geometry for the different sky-viewing measurements.
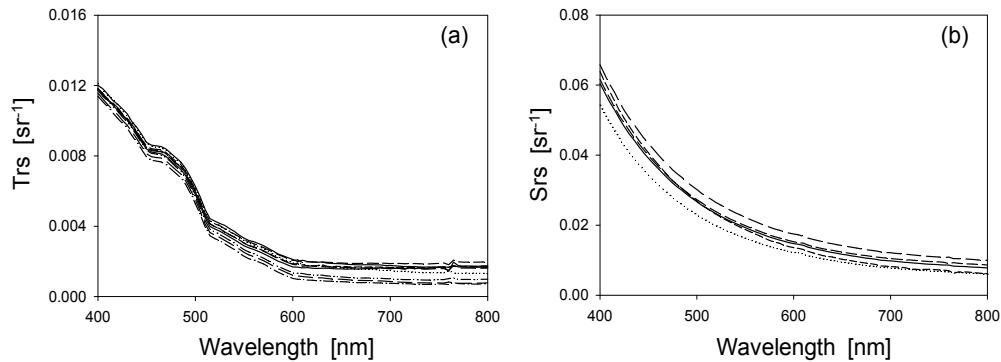

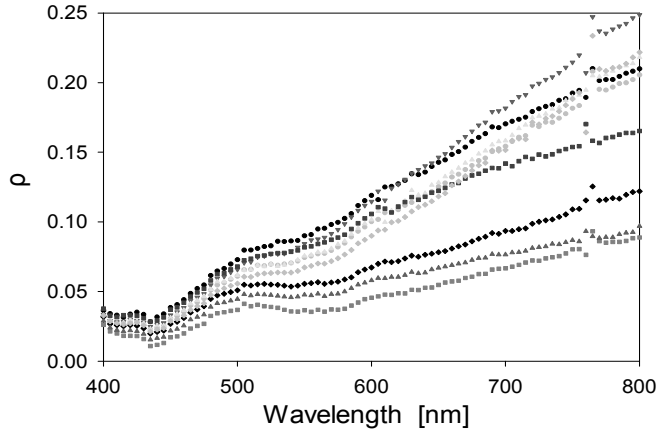Fig. 2. Measured T_{rs} (a) and S_{rs} (b).

Fig. 3. ρ values calculated from measured T_{rs} and S_{rs}. R_{rs} was modeled with Chl = 0.05 mg m^{-3} based on the bio-optical model of Morel and Maritorena [16].

For illustration purposes, Fig. 3 shows values of ρ calculated for the 9 T_{rs} scans and with S_{rs} from the first measurement used as the denominator in Eq. (5). It is seen, not surprisingly, that the ρ values differ among the different L_T measurements. More importantly, the ρ values differ spectrally, and this difference can be as high as a factor of eight between 400 nm and 800 nm (a factor of five between 400 nm and 700 nm). The increase of ρ with wavelength occurs mainly because (1) T_{rs} collects L_{SR} from all directions, including the sun and near-horizon directions [recall the whitish patches in Fig. 1(b)]. Compared to sky light from zenith, radiances from these directions are richer in the longer wavelengths. (2) S_{rs} is measured from one fixed angular geometry, and this S_{rs} is usually blue rich (dominated by contributions from Rayleigh scattering).
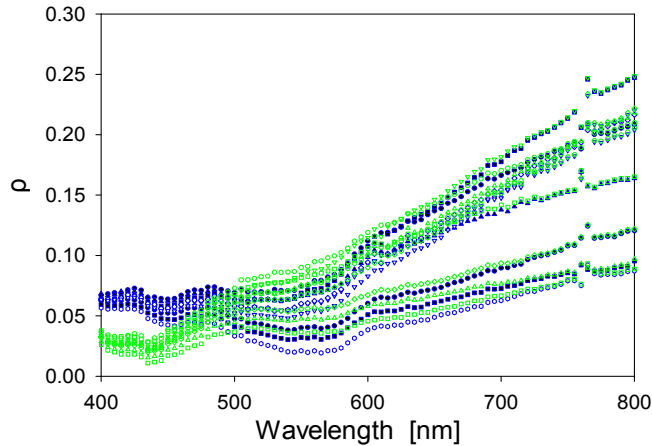

Fig. 4. Similar as Fig. 3, but with two different Chl values. Green: Chl = 0.05 mg m^{-3}; blue, Chl = 0.1 mg m^{-3}.

To evaluate the impacts of incorrect R_{rs}, which were estimated from a spectral model with roughly estimated chlorophyll concentration, on the calculated ρ values, Fig. 4 compares the ρ values calculated from the 9 T_{rs} measurements and the first S_{rs}, but with Chl = 0.05 and 0.1 mg m^{-3}, respectively. For wavelengths in the range of ~400 – 500 nm, because R_{rs} makes strong contributions to T_{rs}, wide variations of ρ values were found, which highlights the limitation of calculating the effective ρ from field measurements when the water contribution

is high. For wavelengths longer than ~550 nm, however, it is found that the impact of different Chl values (then different R_{rs}) on ρ is nearly negligible. This is because for such clear waters phytoplankton contribution to R_{rs} is nearly negligible at the longer wavelengths. This is further illustrated in Fig. 5 via scatter plots between ρ(Chl = 0.05) and ρ(Chl = 0.025), and between ρ(Chl = 0.05) and ρ(Chl = 0.1). This figure shows that Chl has very little impact on ρ values of $\rho > 0.07$ (corresponding to ~550 nm for the measurements in this study). The same results were found when the first S_{rs} was replaced by any of the other measurements of L_{Sky} (results not shown here).
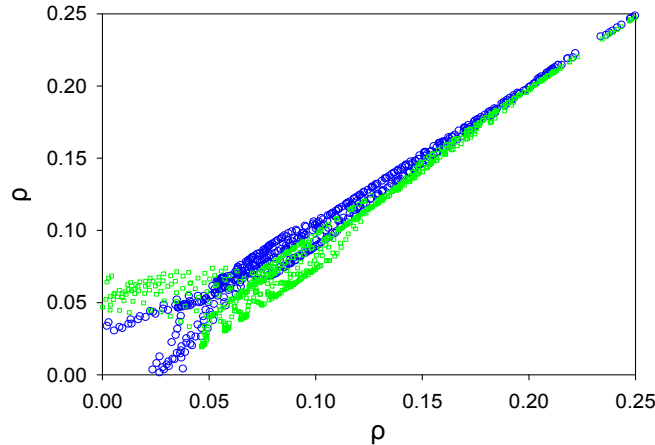

Fig. 5. Scatter plot between ρ(Chl = 0.05) and ρ(Chl = 0.025), blue symbol; and between ρ(Chl = 0.05) and ρ(Chl = 0.1), green symbol.

If there are clouds in the sky (assuming the sun itself is not blocked by clouds), this ρ value could vary widely with wavelength, because S_{rs} could be measured from a small portion of the clear sky (very blue) or aimed at a cloud, while L_{SR} will include radiance from clouds (nearly white) and the background blue sky. These results indicate that applying a ρ value calculated in the near infrared (e.g. 780 nm) to the shorter wavelengths will cause large uncertainties in R_{rs} in the blue bands [2], unless the measurements are made under nearly ideal conditions (no clouds, low wind, no foam on surface, and very short integration time).

4.2 Removal of L_{SR}

The above analysis indicates that when the sea surface is not flat, 1) ρ is not a constant among measurement scans; and 2) ρ values change with wavelength, at least for the longer wavelengths (> ~550 nm) in this study. With such an observation, even if wind speed and angular geometry are all known exactly (note that the effective ρ also depends on the orientation of waves), it will still be a daunting challenge to accurately remove L_{SR} via Eq. (2) or Eq. (4). Earlier, Hooker et al. [2] and Zibordi et al. [4] proposed to filter out the higher L_T measurements before applying Eq. (4b) for the removal of L_{SR}. This technique is generally supported by the results shown in Fig. 3, where higher spectral contrast of ρ is found for the high ρ(800) value (high L_T). However, because it can never be known exactly which L_{Sky} is reflected into the view of an L_T measurement, it is unclear how to select a proper ρ value that is relevant for the smaller L_T measurements, as using the smallest L_T to derive L_W via Eq. (4b) may result in underestimation of L_W [18].

For this station, the wind speed was about 8 m s^{-1}, so a ρ value of 0.05 was assumed for the angular geometry (based on Fig. 8 in Mobley [13]) and applied for the calculation of R_{rs} via Eq. (4). Since there were 9 measurements of T_{rs} and 5 measurements of S_{rs}, 45 R_{rs} were derived. Figure 6 shows the average R_{rs} with ± 1 standard deviation as computed from the 45 spectra. As a qualitative check, the modeled R_{rs} for Chl = 0.05 mg m^{-3} is also included in

Fig. 6. It is found that the average R_{rs} from measurements match modeled R_{rs} reasonably well for the ~400-550 nm range, but there are significant differences for the longer wavelengths. Since there are large uncertainties in the modeled R_{rs} (resulted from, likely, both inaccurate Chl value and imprecise R_{rs} model), we are not expecting the two R_{rs} matching each other exactly. However, because the water-leaving radiance (or R_{rs}) of such waters is nearly negligible at longer wavelengths, it can be safely argued that the R_{rs} derived from Eq. (4) is overestimated for those wavelengths. This observation is consistent with Fig. 13 (left) of Mobley [13].
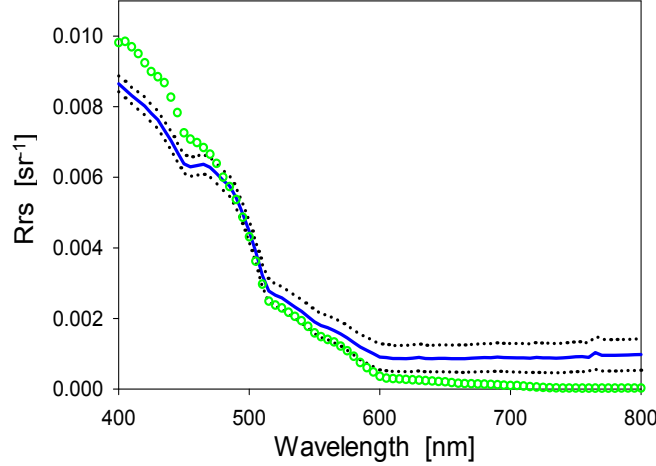

Fig. 6. Average R_{rs} (solid blue) and the one standard deviation (dotted lines), calculated using Eq. (4b). Green line is modeled R_{rs} with Chl = 0.05 mg m^{-3} using the Morel-Maritorena bio-optical model [16].

The commonly measured properties (except grey card) are L_T at angle (θ, φ) and L_{Sky} at (θ', φ). Also, because the actual total L_{SR} is not measured directly, we re-write Eq. (1) as

$$L_T(\lambda, \theta, \varphi) = L_W(\lambda, \theta, \varphi) + w_0 F(\theta, \varphi) L_{Sky}(\lambda, \theta', \varphi) + \sum_{i-1} w_i F(\theta_i', \varphi_i', \theta, \varphi) L_{Sky}(\lambda, \theta_i', \varphi_i').$$

(6)

Here w_0 represents the weighting of sky light coming from the specular direction (θ', φ), and the sum now includes sky light from all other directions. Further, since sky light from the specular direction (θ', φ) dominates L_{SR} from the field-of-view centered at (θ, φ) [13], Eq. (6) is approximated (by setting $w_0 = 1$) as,

$$L_T(\lambda, \theta, \varphi) \approx L_W(\lambda, \theta, \varphi) + F(\theta, \varphi) L_{Sky}(\lambda, \theta', \varphi) + \sum_{i-1} w_i F(\theta_i', \varphi_i', \theta, \varphi) L_{sky}(\lambda, \theta_i', \varphi_i'),$$

(7)

or, in terms of reflectance,

$$T_{rs}(\lambda, \theta, \varphi) \approx R_{rs}(\lambda, \theta, \varphi) + F(\theta, \varphi) S_{rs}(\lambda, \theta', \varphi) + \sum_{i-1} w_i F(\theta_i', \varphi_i', \theta, \varphi) S_{rs}(\lambda, \theta_i', \varphi_i').$$

(8)

Now in Eq. (8) both T_{rs} and S_{rs} for the specular direction are directly determined from measurements. $F(\theta, \varphi)$ is the Fresnel reflectance of water surface for (θ, φ), which is known for a given angular geometry. For the calculation of R_{rs} from Eq. (8) for any measurement of L_T and L_{Sky}, it is thus necessary to determine the last term on the right-hand side of Eq. (8).

Because it is not known yet how this last term varies spectrally, this term is assumed for expediency to be spectrally independent [9]. Thus Eq. (8) becomes

$$T_{rs}(\lambda,\theta,\varphi) \approx R_{rs}(\lambda,\theta,\varphi) + F(\theta,\varphi)\,S_{rs}(\lambda,\theta',\varphi) + \Delta(\theta,\varphi), \qquad (9a)$$

or [9],

$$R_{rs}(\lambda,\theta,\varphi) \approx T_{rs}(\lambda,\theta,\varphi) - F(\theta,\varphi)\,S_{rs}(\lambda,\theta',\varphi) - \Delta(\theta,\varphi). \qquad (9b)$$

Thus, for each set of spectral T_{rs} and S_{rs}, there is a spectrally constant value (Δ, a bias) that must be determined before R_{rs} can be derived. For oceanic waters where R_{rs} is negligible in the red and near infrared, Δ can be estimated by assuming R_{rs} near 750 nm is 0 [19]. For coastal turbid waters, however, this assumption is no longer valid. For such environments, one approach [19,20] is to model the spectral R_{rs} as a function of spectral inherent optical properties (IOPs), and then solve for Δ by comparing modeled spectral R_{rs} with spectral R_{rs} derived from Eq. (9b) using all measured spectral information (so-called spectral optimization) [21–24].

Basically, for optically deep waters, the spectral R_{rs} can be conceptually summarized as

$$R_{rs}(\lambda,\theta,\varphi) \approx Fun(a(\lambda), b_b(\lambda), \theta, \varphi), \qquad (10)$$

where $a(\lambda)$ is the absorption coefficient, and $b_b(\lambda)$ is the backscattering coefficient. The inherent optical properties $a(\lambda)$ and $b_b(\lambda)$ can be modeled with bio-optical models of optically active components [22,24,25], so that Eq. (10) becomes explicit functions as

$$\begin{cases} R_{rs}(\lambda_1,\theta,\varphi) \approx Fun(a_w(\lambda_1), b_{bw}(\lambda_1), P, G, X, \theta, \varphi), \\ R_{rs}(\lambda_2,\theta,\varphi) \approx Fun(a_w(\lambda_2), b_{bw}(\lambda_2), P, G, X, \theta, \varphi), \\ \quad . \\ R_{rs}(\lambda_n,\theta,\varphi) \approx Fun(a_w(\lambda_n), b_{bw}(\lambda_n), P, G, X, \theta, \varphi). \end{cases} \qquad (11)$$

Here λ_1 to λ_n are the sensor's wavelengths, a_w and b_{bw} are the known absorption and backscattering coefficients of pure seawater, and P, G, and X represent the magnitude of the absorption coefficient of phytoplankton, gelbstoff, and the backscattering coefficient of particles, respectively. To derive the value of Δ in Eq. (9b), an objective function is defined as

$$Err = \frac{\left[\bigcup_{400}^{675}\left(R_{rs} - \tilde{R}_{rs}\right)^2 + \bigcup_{750}^{800}\left(R_{rs} - \tilde{R}_{rs}\right)^2\right]^{0.5}}{\bigcup_{400}^{675} R_{rs} + \bigcup_{750}^{800} R_{rs}}, \qquad (12)$$

with $\tilde{R}_{rs}$ from Eq. (11) while R_{rs} from Eq. (9b). $\bigcup_{400}^{675}$ represents the average of an array between 400 nm and 675 nm. The upper bound of wavelength (800 nm) can be extended to a longer wavelength for turbid lake or river waters when sensor has measurements in those wavelength ranges. *Err* is then a function of 4 variables (*P, G, X,* and Δ) for optically deep waters, and they are derived numerically when *Err* reaches a minimum – spectral optimization [22,26]. R_{rs} is therefore computed by applying this numerically derived Δ to Eq. (9b). Note that in the correction of L_{SR} the focus is the estimation of Δ, although values of *P, G,* and *X* are also determined.

For the measurements at this station, again, 45 spectral R_{rs} were determined with this spectral optimization method, and their average and standard deviation are presented in Fig. 7. The overestimations of R_{rs} in the longer wavelengths (> ~550 nm) are generally removed, as compared to Fig. 6. At the same time, the average R_{rs} matches the modeled R_{rs} (with Chl = 0.05 mg m^{-3}) very well in the ~400-550 nm range, although it is not our intension (the measured and Chl-modeled R_{rs} do not necessarily represent the same water environments).
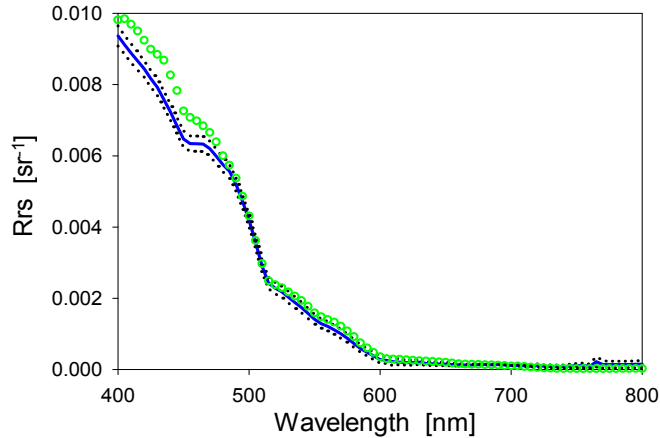
Fig. 7. Similar as Fig. 6, but R_{rs} was calculated based on Eq. (9) and with a spectral optimization scheme. Green line is modeled R_{rs} with Chl = 0.05 mg m^{-3} using the Morel-Maritorena [16] bio-optical model.

To further test the above evaluation and the optimization approach of removing L_{SR}, new measurements (September 13, 2010; ~11 am local time) were carried out (with SPECTRIX) over turbid river water (Pearl River, Mississippi, USA. Figure 8 shows color photos of the water and sky when measurements were taken). This shallow (~0.5 m) and very turbid water makes it nearly impossible to obtain R_{rs} from measurements of vertical profiles of L_u and E_d [6]. During the experiment, the surface was calm [see Fig. 8(a)] and the sky was blue [Fig. 8(b)] with some thin cirrus clouds. Two different measurement schemes were carried out. One followed the traditional scheme [10] that measures L_G, L_T and L_{Sky} (see Section 3), with θ = 30° from nadir and φ = 90° from the solar plane, and the sensor to water-surface distance was ~1 meter (the sensor then covered a surface area ~0.05 m^2). R_{rs} were derived, separately, from these measurements following the simple approach [Eq. (4b), ρ = 0.022 is used for calm surface. R_{rs}-*simp* in the following] and following the optimization approach (R_{rs}-*opt* in the following) mentioned above.
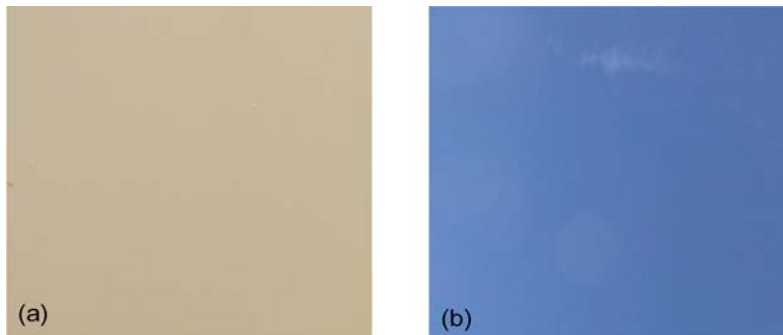

Fig. 8. Color photos of the river water (a) and sky (b) measured on September 13, 2010, ~11 am local time.

Another measurement followed a novel scheme proposed by Ahn et al [27], where a small black tube (~4 cm in diameter) was placed in front of the sensor to block L_{SR} (see Fig. 9 for a schematic illustration). When L_T was measured the tube was dipped just below the sea surface (~5 cm) while the sensor itself was kept above the surface. Therefore there will be no L_{SR} into the sensor in this setup and the instrument records a direct measurement of L_W. R_{rs} (R_{rs}-*direct* in the following) was then derived as the ratio of measured L_W to E_d (from measurement of L_G).
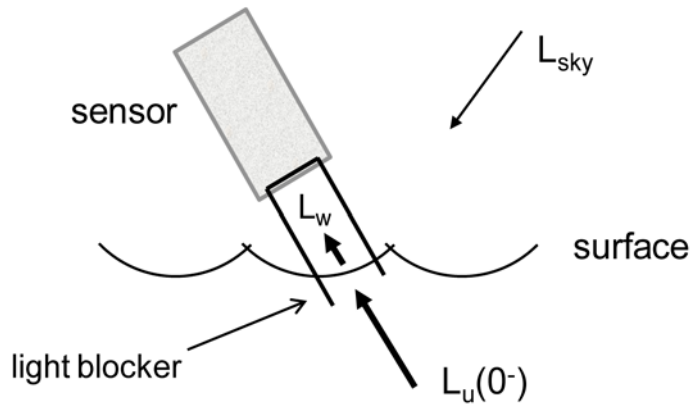
Fig. 9. Scheme to measure L_W directly (re-drawn from Ahn et al [27]). The open box is a black tube to block surface reflected light, which is inserted just below (~5 cm) the surface when measuring L_W.

Figure 10 shows the derived R_{rs} from the three measurement-determination schemes; blue is R_{rs}-*direct*, green is R_{rs}-*opt*, and cyan is R_{rs}-*simp*. The three R_{rs} curves show similar spectral shapes, which are typical of turbid, high-CDOM river waters (note the yellow-brown color in Fig. 8). R_{rs}-*simp* is considerably higher than both R_{rs}-*direct* and R_{rs}-*opt*, suggesting incomplete removal of L_{SR} even for this quite calm situation (it may be that some sun glitter could not be completely avoided for the (30°,90°) viewing geometry and integration times of ~1-2 seconds). On the other hand, R_{rs}-*direct* and R_{rs}-*opt* are very consistent across the ~400-850 nm range, with a coefficient of variation about ~11% (which is about 46% between R_{rs}-*simp* and R_{rs}-*direct*). The slight negative R_{rs} (both R_{rs}-*direct* and R_{rs}-*opt*) for wavelengths shorter than 400 nm may result from a combination of 1) SPECTRIX has lower signal-to-noise ratio for wavelengths shorter than ~400 nm [15], and 2) the extremely low upwelling signal in the blue-to-UV wavelengths of this CDOM-rich water. Nevertheless, the deduced R_{rs} of this turbid water (along with the result of blue oceanic waters) strongly indicates that Eq. (9b) with an optimization scheme to determine the value of Δ is adequate in obtaining R_{rs} in the field when measurements are made above the sea surface under un-ideal conditions and that L_{SR} is not blocked during measurements. However, neither R_{rs}-*direct* nor R_{rs}-*opt* are error free, because R_{rs}-*direct* encounters some self-shading and/or contributions from reflectance inside the tube, while R_{rs}-*opt* suffers from the approximation from Eq. (6) to Eqs. (7) and (9a).
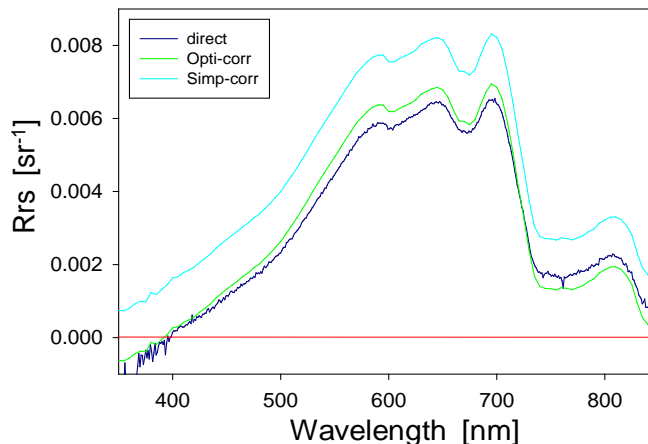

Fig. 10. Comparison between directly measured R_{rs} (blue line) of water showing in Fig. 8(a) and R_{rs} obtained after correcting surface-reflected light.

5. Conclusions

Using measurements from a clear-water station, we demonstrated that the effective surface reflectance (ρ) varies not only with each measurement scan but also with wavelength. Consequently, application of a spectrally constant ρ value for the removal of L_{SR} from above-surface measurements is a crude approximation, especially if the sea surface is significantly roughened by waves and the sensor has a long integration time (as do most high-spectral resolution sensors). Earlier studies [2,4,18] have shown that it is wise to filter out the higher L_T measurements before the derivation of L_W when the simple formula [e.g., Eq. (4b)] is used for the derivation. Here we show that for clear to turbid waters, a spectral optimization scheme [28] is also adequate to remove L_{SR} in L_T measurements and derive reasonable R_{rs}. Further, the scheme to block L_{SR} by equipping a black tube in front of the sensor and dipping it just below the surface shows promise to obtain reliable measurement of L_W without the difficult post-processing. Further effort is required by the remote-sensing community to evaluate these approaches for a wide range of environments and measurement conditions (e.g. Hooker et al. [2] and Toole et al [7]) and then to establish a consensus for the optimum way to determine R_{rs} in the field when measurements are made from an above-surface platform, especially for situations such as turbid waters and partly cloudy skies.

Acknowledgements